A multifrequency study of the active star-forming complex NGC 6357 – I. Interstellar structures linked to the open cluster Pis 24

C. E. Cappa,[1,2]★ R. Barbá,[3,4] N. U. Duronea,[1] J. Vasquez,[1,2] E. M. Arnal,[1,2]
W. M. Goss[5] and E. Fernández Lajús[2,6]

[1]*Instituto Argentino de Radioastronomía (CCT-La Plata, CONICET), C.C. No. 5, 1894 Villa Elisa, Argentina*
[2]*Facultad de Ciencias Astronómicas y Geofísicas, Universidad Nacional de La Plata, Paseo del Bosque s/n, 1900 La Plata, Argentina*
[3]*Instituto de Ciencias Astronómicas, de la Tierra y del Espacio (ICATE-CONICET), Av. España Sur 1512, J5402DSP San Juan, Argentina*
[4]*Departamento de Física, Universidad de La Serena, Cisternas 1200 Norte, La Serena, Chile*
[5]*National Radio Astronomy Observatory, PO Box 0, Socorro, NM 87801, USA*
[6]*Instituto de Astrofísica de La Plata (IALP-CONICET), Paseo del Bosque s/n, 1900 La Plata, Argentina*

ABSTRACT

We investigate the distribution of gas (ionized, neutral atomic and molecular) and interstellar dust in the complex star-forming region NGC 6357 with the goal of studying the interplay between the massive stars in the open cluster Pis 24 and the surrounding interstellar matter.

Our study of the distribution of the ionized gas is based on narrow-band Hα, [S II]and [O III] images obtained with the Curtis–Schmidt Camera at CTIO, Chile, and on radio continuum observations at 1465 MHz taken with the VLA with a synthesized beam of 40 arcsec. The distribution of the molecular gas is analysed using ^{12}CO(1−0) data obtained with the NANTEN radiotelescope, Chile (angular resolution = 2.7 arcmin). The interstellar dust distribution was studied using mid-infrared data from the GLIMPSE survey and far-infrared observations from *IRAS*.

NGC 6357 consists of a large ionized shell and a number of smaller optical nebulosities. The optical, radio continuum, and near- and mid-IR images delineate the distributions of the ionized gas and interstellar dust in the H II regions and in previously unknown wind-blown bubbles linked to the massive stars in Pis 24 revealing surrounding photodissociation regions. The CO line observations allowed us to identify the molecular counterparts of the ionized structures in the complex and to confirm the presence of photodissociation regions. The action of the WR star HD 157504 on the surrounding gas was also investigated. The molecular mass in the complex is estimated to be $(4 \pm 2) \times 10^5$ M$_\odot$. The mean electron densities derived from the radio data suggest electron densities >200 cm^{-3}, indicating that NGC 6357 is a complex formed in a region of high ambient density. The known massive stars in Pis 24 and a number of newly inferred massive stars are mainly responsible for the excitation and photodissociation of the parental molecular cloud.

Key words: H II regions – ISM: bubbles – ISM: individual objects: NGC 6357 – open clusters and associations: individual: Pis 24.

1 INTRODUCTION

NGC 6357 ($\equiv$ W 22 $\equiv$ RCW 131 $\equiv$ Sh2-11) is a large H II complex located in the Sagittarius spiral arm. The H II complex consists of an incomplete large shell of about 60 arcmin in diameter, many other bright optical nebulosities in different evolutionary stages, many OB stars belonging to the open cluster Pis 24, and bright infrared (IR) sources, some of them young stellar object (YSO) candidates

(Lortet, Testor & Niemela 1984; Felli et al. 1990; Bohigas et al. 2004; Wang et al. 2007; Russeil et al. 2010).

Lortet et al. (1984) showed that the large shell was a low-excitation and ionization-bounded H II region. This shell, which can also be identified in images in the mid-IR (Wang et al. 2007), opens to the north. The shell shows no evidence of expansion motions in optical lines (Lortet et al. 1984) and has been interpreted as an ionized gas bubble created by the strong winds of the current massive stars in Pis 24 or by a previous generation of stars (Lortet et al. 1984; Bohigas et al. 2004; Wang et al. 2007).

★E-mail: ccappa@fcaglp.fcaglp.unlp.edu.ar

The two brightest H II regions in the complex are G353.2+0.9 and G353.1+0.6. G353.2+0.9 is the brightest region at optical and radio wavelengths (e.g. Felli et al. 1990). Both the extended radio sources were detected at several frequencies (e.g. Shaver & Goss 1970; Haynes, Caswell & Simons 1978). Detailed studies of these two bright regions were performed using VLA observations at 5 GHz with an angular resolution of 10.0 arcsec (Felli et al. 1990). Optical images of the whole NGC 6357 region show a number of additional ionized regions on which no optical and radio studies were previously carried out.

The distribution of the molecular gas associated with selected regions in the complex was investigated by McBreen, Jaffe & Fazio (1983) and Massi, Brand & Felli (1997). The latter authors found that the bulk of the molecular gas related to the complex has velocities in the range of $[-14, +4]$ km s^{-1}.

The massive open cluster Pis 24, which lies in the central cavity of NGC 6357 and has an age of about 2×10^6 yr, is considered to be the only ionization source of the complex because of the huge number of UV photons emitted by the massive stars (Massey, DeGioia-Eastwood & Waterhouse 2001). The cluster contains at least a dozen O-type stars (Wang et al. 2007), including two of the most luminous stars known in the Galaxy (Bohigas et al. 2004). These stars were classified as O3.5If (Pis 24-1) and O3.5III(f*) (Pis 24-17) by Walborn et al. (2002). Recent studies by Maíz Apellániz et al. (2007) showed that Pis 24-1 is a multiple system. The Wolf–Rayet star WR 93 ($\equiv$HD 157406, WC7 + O7-9, van der Hucht 2001) is also projected on to this region. Massey et al. (2001) consider this star to be a probable member of the cluster. However, the large uncertainties in reddening and distance determinations cast doubts on its relation to the cluster. In addition to the visible stars, massive OB stars hidden in areas with high reddening may also contribute to the ionization and photodissociation of the gas (Felli et al. 1990).

The study by Persi et al. (1986) of this region focused on stellar formation activity. This study, along with more recent searches for YSOs in the region, resulted in the discovery of objects ranging from a large number of infrared and X-ray source candidates to YSOs and massive stars with high reddening (e.g. Bohigas et al. 2004; Wang et al. 2007), showing that the whole H II complex is an active area of recent and on-going star formation.

Distance determinations to the ionized complex span the range 1.7–2.6 kpc. Neckel (1978) and Lortet et al. (1984) derived a distance of 1.7 kpc from UBV and Hβ data, and from the nebular reddening, respectively. Massey et al. (2001), based on recent spectral classification and absolute magnitude calibration, redetermined the distance to Pismis 24, adopting $(m-M)_o = 12.0$ mag, or $d = 2.5$ kpc. Following Massey et al. (2001), we adopt a distance $d = 2.5 \pm 0.5$ kpc for the H II complex.

With the aim of investigating the interplay between the massive stars belonging to Pis 24 and the different components of the neighbouring interstellar material, we analysed Hα, [O III] and [S II] images obtained at CTIO, VLA radio continuum observations at 1.465 GHz, and CO(1−0) observations obtained using the NAN-TEN telescope, as well as *IRAS* archive images (*IRAS*–HIRES) at 60 and 100 μm, and GLIMPSE IRAC archive images in the near- and mid-IR. Optical line ratios are extremely useful in investigating the excitation conditions in different areas of the complex. High-resolution radio images lead to the distribution of ionized gas in highly obscured regions, and in the derivation of the physical parameters of ionized regions. Images in the mid- and far-infrared lead to the characterization of the interstellar dust in the complex. As a substantial amount of molecular gas is expected to be present

in star-forming regions, we also observed the whole complex in the CO(1−0) line at 115 GHz.

This is the first of a series of papers dealing with this complex. This paper focuses on some of the most interesting structures in the complex, excited by the massive stars in the open cluster Pis 24. The bright regions G353.24+0.64 and G353.1+0.6 will be analysed in a subsequent paper.

Our study provides new information about the interstellar dust, and the ionized and neutral gas distributions in the complex and the dust and gas masses. Interstellar bubbles, H II regions and photodissociation regions (PDRs) excited by known members of the open cluster Pis 24 and newly inferred massive stars in the complex are revealed.

2 OBSERVATIONS

2.1 Optical images

Narrow-band [O III], Hα and [S II], and broad-band *V* and *R* CCD images were obtained on 1999 May, using the Curtis–Schmidt Camera at Cerro Tololo Inter-American Observatory (CTIO), Chile. The camera was equipped with a Site2K 2048 × 2048 array and has a pixel scale of 2.3 arcsec pixel^{-1}. The seeing during observations was typically about 1 arcsec giving a pronounced undersampling for point sources. The narrow-band images were obtained with filters[1] centred at 5027, 6567, and 6744 Å, with an FWHM of about 50, 68 and 50 Å, respectively. The Hα filter also includes some contamination of neighbouring [N II] nebular emission lines at 6548 and 6584 Å.

The individual images in each filter were corrected by bias level and flat-field, and then combined into a single mosaic using IRAF routines.[2] These mosaics were registered by using hundreds of stars in the overlapping region. For each final mosaic an astrometric solution was found using stellar positions derived from the Guide Star Catalog 2.0. The absolute coordinate accuracy for each mosaic is better than 0.4 arcsec, although the typical relative uncertainty in the registration between images has been reduced to less than 0.1 pixels.

The surface brightness calibration process was performed using narrow-band images of Pis 24 obtained with the Advanced Camera for Surveys (ACS) and the Wide Field and Planetary Camera 2 (WFPC2) on board the *Hubble Space Telescope* (*HST*). The data sets correspond to those obtained by Observing Programs No. 9857 (PI: O. De Marco) and No. 9091 (PI: J. Hester) for ACS and WFPC2 instruments, respectively. The ACS/WFC filter F658N ($\lambda_c \sim 6584$, FWHM ~ 73 Å) has similar characteristics as the Hα filter used in the Curtis–Schmidt camera. The WFPC2 filters F673N ($\lambda_c \sim 6732$, FWHM ~ 65 Å) and F502N ($\lambda_c \sim 5012$, FWHM ~ 37 Å) have also similar characteristics as the [S II] and [O III] filters used in the Curtis–Schmidt Camera. The relative surface brightness zero-points were obtained using two areas of about 30 arcsec in common with ACS and WFPC2 images. Uncertainties in the relative calibrations for the Curtis–Schmidt filters are below 20 per cent. This figure is derived from the comparison of measurements in adjacent areas.

---

[1] Passbands are plotted in
http://www.ctio.noao.edu/instruments/filters/filters$_{34}$.html
[www.ctio.noao.edu]
[2] IRAF is distributed by the National Optical Observatories which is operated by the Association of Universities for Research in Astronomy, Inc., under cooperative agreement with the National Science Foundation.

2.2 Radio images

2.2.1 Radio continuum at 1.46 GHz

The distribution of the ionized gas was also investigated using radio continuum data. The surveyed field, which corresponds to the central region of the complex, was observed at 1.465 MHz (20 cm) using the Very Large Array in the DnC configuration on 2000 July 3 and 5 as part of the AC555 observing programme. The sources 1328+307 ($\equiv$3C 286l, $S_{1.46\,GHz}$ = 14.9 Jy) and 1748−253 ($S_{1.46\,GHz}$ = 1.3 Jy) were used as primary and secondary flux density calibrators, respectively. The bandwidth was 50 MHz and the total integration time 2 h. The coordinates of the field centre are $17^h25^m8\overset{s}{.}56$, $-34°11'13\overset{''}{.}04$ (J2000). The synthesized beam is 43.9 × 34.3 arcsec^2 at a position angle of +41y°.

The data were edited, calibrated, self-calibrated and imaged using AIPS tasks. The rms in the central part of the image is 20 mJy beam^{-1}.

2.2.2 CO line data

Intermediate angular resolution and medium-sensitivity CO data were obtained with the 4-m NANTEN millimetre-wave telescope of Nagoya University. At the time of the observations this telescope was installed at the Las Campanas Observatory, Chile. The half-power beamwidth and the system temperature, including the atmospheric contribution towards the zenith, were 2.6 arcmin and ∼220 K (SSB) at 115 GHz.

The data were gathered using the position-switching mode. Observations of points devoid of CO emission were interspersed among the programme positions. The coordinates of these points were retrieved from a data base that was kindly made available to us by the NANTEN staff. The spectrometer used was an acusto-optical with 2048 channels providing a velocity resolution of ∼0.055 km s^{-1}. For intensity calibrations, a room-temperature chopper wheel was employed (Penzias & Burrus 1973). An absolute intensity calibration was achieved by observing Orion KL (RA,Dec. [J2000] = $5^h40^m14\overset{s}{.}5$, $-5°22'49\overset{''}{.}3$) and ρ Oph East (RA,Dec. [J2000] = $16^h32^m22\overset{s}{.}8$, $-24°28'33\overset{''}{.}1$). The absolute radiation temperature, T_R^*, of Orion KL and ρ Oph East were assumed to be 65 and 15 K, respectively (Ulich & Haas 1976; Kutner & Ulich 1981).

The CO observations were carried out in 2001 April and the surveyed area is defined by $352°51 \leq l \leq 353°95$ and $0°14 \leq b \leq 1°58$.[3] An inner area defined by $352°96 \leq l \leq 353°50$ and $0°59 \leq b \leq 1°13$ was sampled[4] at one beamwidth intervals, while the remaining area was sampled every 5.4 arcmin (two beamwidths). The total number of observed pointings is 349. The integration time per pointing was 16 s resulting in a typical rms noise of $\Delta T_{rms} \sim$ 0.34 K.

2.3 Infrared data

The warm dust distribution was analysed using high-resolution (HIRES) *IRAS* data obtained through *IPAC*.[5] The IR data in the

---

[3] In equatorial coordinates, the four vertices of this region are RA,Dec. (J2000) = $(17^h25^m58\overset{s}{.}21$, $-35°10'4\overset{''}{.}4)$, $(17^h20^m11\overset{s}{.}26$, $-34°21'9\overset{''}{.}8)$ $(17^h24^m6\overset{s}{.}94$, $-33°10'1\overset{''}{.}8)$, and $(17^h29^m51\overset{s}{.}35$, $-33°58'10\overset{''}{.}7)$.

[4] The four vertices of this region are RA,Dec. (J2000) = $(17^h25^m22\overset{s}{.}9$, $-34°32'32\overset{''}{.}0)$, $(17^h23^m13\overset{s}{.}09$, $-34°14'17\overset{''}{.}7)$, $(17^h24^m41\overset{s}{.}19$, $-33°47'32\overset{''}{.}1)$, and $(17^h26^m50\overset{s}{.}64$, $-34°5'40\overset{''}{.}4)$.

[5] *IPAC* is funded by NASA as part of the *IRAS* extended mission under contract to Jet Propulsion Laboratory (JPL) and California Institute of Technology (Caltech).

IRAS bands at 60 and 100 μm have angular resolutions of 1.5 and 1.7 arcmin.

High angular resolution IRAC images from the Galactic Legacy Infrared Mid-Plane Survey Extraordinaire (GLIMPSE; Benjamin et al. 2003) at 3.6 μm (with angular resolution ϕ = 1.5 arcsec), 4.5 μm (ϕ = 1.7 arcsec), 5.8 μm (ϕ = 1.8 arcsec) and 8.0 μm (ϕ = 1.94 arcsec) obtained with *Spitzer* were also used. Additional information on IRAC images is available from Fazio et al. (2004) and from the Spitzer Science Center Observer Support Website.[6]

3 GENERAL CHARACTERISTICS OF THE COMPLEX

In this section we describe the general distribution of the ionized and neutral gas, while a detailed analysis of some of the most interesting regions will be discussed in the following sections.

Fig. 1 shows a composite image of NGC 6357. Hα is shown in green, [O III] in blue and [S II] in red. The filamentary structure of the ionized gas is evident. In addition to the large shell, clearly detected in Hα and [S II] emissions, the complex shows numerous shell-like features, dust lanes and globules. In Fig. 2 we indicate the location of the most prominent features to facilitate their identification. The known H II regions G353.2+0.9 and G353.1+0.6, the large shell, and a number of other interesting optical structures, like G353.12+0.86 and G353.24+0.64, are indicated in Fig. 2. An elongated structure at RA,Dec.(J2000) = $17^h24^m30^s$, $-34°5'$ (referred to as Structure 1), an optical filament probably linked to WR 93, and the positions of WR 93 and Pis 24 are also indicated in this figure.

In this paper we investigate the characteristics of the H II region G353.2+0.9 and those of the ionized shell G353.12+0.86 and the large shell including Structure 1. The prominent regions G353.1+0.6 and G353.24+0.64 will be analysed in a subsequent paper.

Figs 3 and 4 show the [S II]/Hα and [O III]/Hα line ratios. Based on the different excitation conditions, these images provide the evidence to distinguish whether the sources are H II regions, interstellar bubbles or PDRs. Low [S II]/Hα and [O III]/Hα line ratios are indicative of low-excitation conditions associated with H II regions such as the large shell; on the other hand, higher [O III]/Hα line ratios can be associated with interstellar bubbles. In this context, G353.12+0.86 is a stellar wind bubble.

Fig. 5 displays the VLA image at 1.46 GHz, which covers most of the complex. A comparison with the optical images reveals the radio continuum counterparts of most of the optical features indicated in Fig. 2. In particular, the brightest H II regions G353.2+0.9 and G353.1+0.6, which were studied by Felli et al. (1990) at 5.0 GHz, are easily identified. On the contrary, G353.2+0.7 (centred at $17^h25^m35.52^s$, $-34°16'54\overset{''}{.}6$), which was also investigated by Felli et al. (1990), cannot be identified in the radio continuum image as a distinct physical structure. The western border of this feature, as delineated by Felli et al. (1990), is part of G353.12+0.86, while the eastern section may be part of G353.24+0.64 or of the large shell, as pointed out by Felli et al. (1990). The radio counterpart of the shell-like structure G353.12+0.86 is first identified. The radio-emitting region at 17^h25^m, $-34°12'20''$, located slightly to the south-east of the H II region G353.2+0.9, lacks an optical counterpart.

---

[6] Available at http://ssc.spitzer.caltech.edu/ost
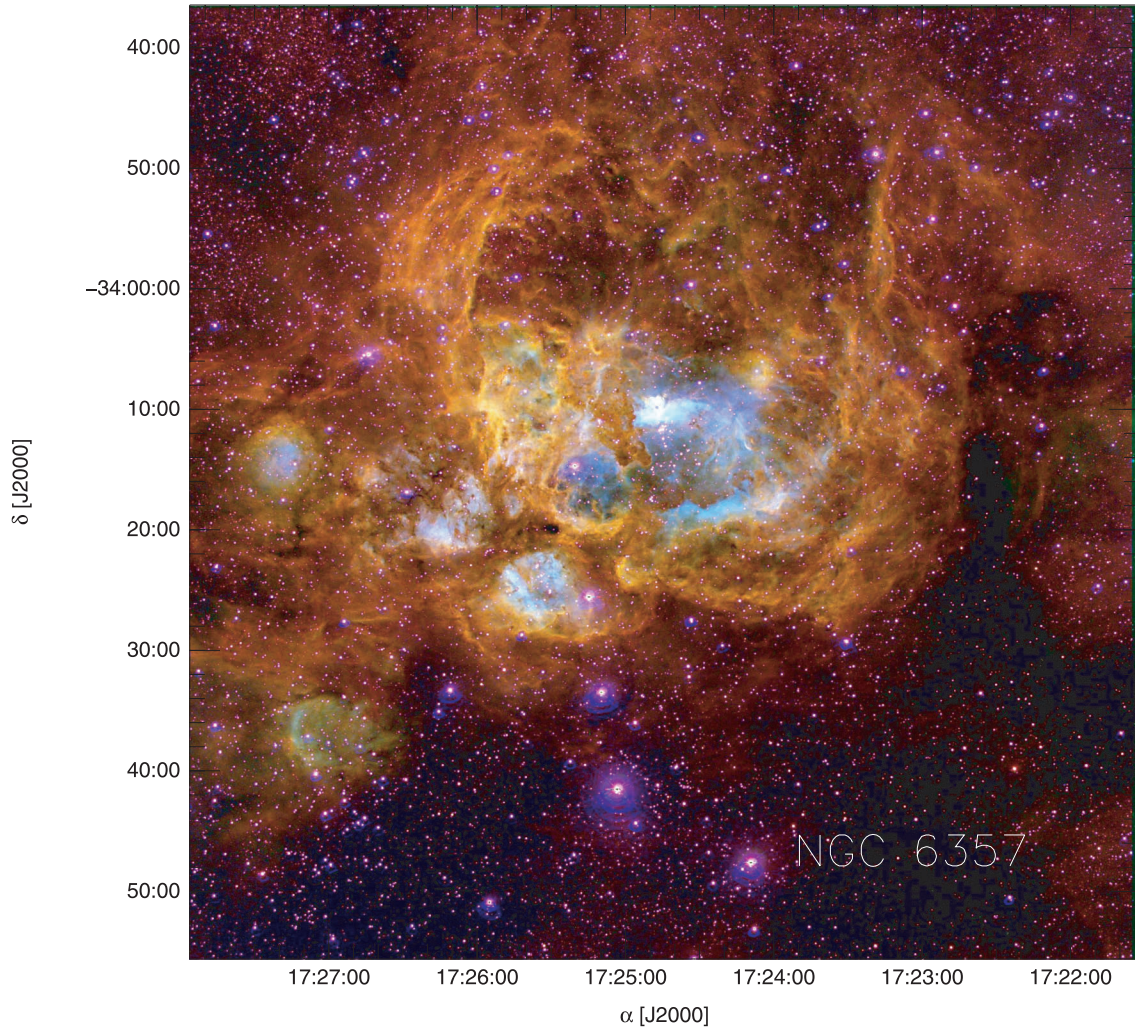
Figure 1. Colour composite image of NGC 6357. Red, green and blue show emission from [S II] 6716-31 Å, Hαand [O III] 5007 Å, respectively. These images were obtained with the Curtis–Schmidt camera at CTIO during 1999.

The upper panel of Fig. 6 shows the distribution of the dust colour temperature T_c (in contours and grey-scale), while an overlay of the Hα emission distribution (in grey-scale) and T_c (in contours) is displayed in the lower panel. The dust colour temperature distribution was obtained from the *HIRES* images at 60 and 100 μm, following the procedure described by Cichowolski et al. (2001). Derived temperatures correspond to $n = 1.5$. The parameter n is related to the dust absorption efficiency ($\kappa_\nu \propto \nu^n$). We adopted $\kappa_\nu = 40\,\text{cm}^2\,\text{g}^{-1}$, a value derived from the expressions by Hildebrand (1983). Dust temperatures range from ∼25 to ∼50 K, with the highest values close to G353.2+0.9, in agreement with previous results from Persi et al. (1986). The region of low dust temperatures at $17^h25^m15^s$, $-34°18'$, encircled by regions with higher temperatures, coincides with the eastern section of the cavity of G353.12+0.86. Dust linked to the W arm of the large shell has a dust temperature of 30 K, while values as high as 50 K were derived for the environs of G353.2+0.9. Regions with high T_c far from Pis 24 (for example G353.1+0.6) are suggestive of the existence of unknown excitation sources (Damke, Barbá & Morrell 2006).

The derived dust temperatures are typical of H II regions. A comparison with the optical image shows that areas with high dust temperature coincide with bright Hα or radio continuum emitting regions. This behaviour is compatible with the fact that the stellar UV radiation field of the massive stars in the region is responsible for the heating of the interstellar dust.

Fig. 7 displays a composite image of the brightest areas of NGC 6357 using the IRAC images: 3.6 μm is in blue, 4.5 μm in green and 8 μm in red. Emission at 3.6 μm originates in a faint and diffuse PAH feature at 3.3 μm and in dispersed stellar light; the 4.5-μm band shows emission from Brα and Pfβ and vibrational H_2 lines and rotovibrational CO lines, typical of shocked gas (e.g. Churchwell et al. 2006; Watson et al. 2008). Emission at 8 μm includes strong features from polycyclic aromatic hydrocarbons (PAHs), which are prominent. PAH emission and ionized gas emission (shown by the Hα and 1.46 GHz images) have different spatial distributions, with the ionized gas located in the inner area of the structures, closer to the excitation sources than PAH emission. PAHs cannot survive inside H II regions (Cesarsky et al. 1996), but they do on neutral PDRs at the interface between ionized and molecular gas. Thus, the emission at 8 μm shows that PDRs are widespread in this complex, a characteristic also indicative of the presence of molecular gas. PDRs are clearly delineated in this image (areas in
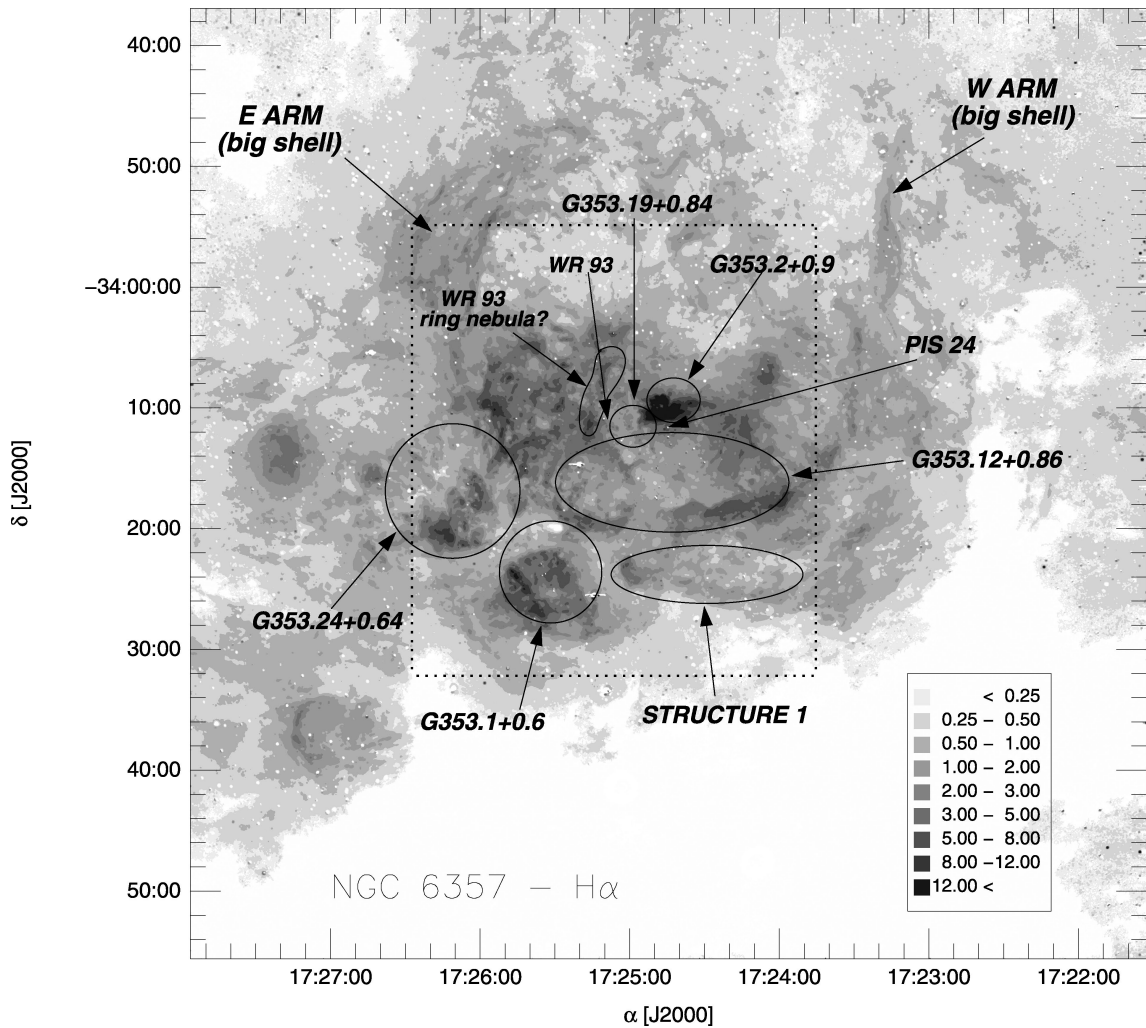
Figure 2. Continuum-subtracted Hα image of NGC 6357 obtained at CTIO. Different structures in the ionized complex are indicated to facilitate their identification in Fig. 1. The grey-scale values are in the unit of $10^{-14}\,\mathrm{erg\,cm^{-2}\,s^{-1}\,pix^{-1}}$. The dotted line delineates the region observed at 1.46 GHz.

magenta and white). The detection of CI radio recombination lines from several areas in NGC 6357 is also indicative of the presence of PDRs (Quireza et al. 2006). The emission at 4.5 μm, coincident with the PDRs (detected at 8 μm), probably indicates the presence of shocked gas in these last regions. The brightest region in all of the IRAC bands is G353.2+0.9.

Elephant trunks are present throughout the region. Clear examples are located at $17^{\mathrm{h}}25^{\mathrm{m}}00^{\mathrm{s}}$, $-34°14'$ and at $17^{\mathrm{h}}24^{\mathrm{m}}50^{\mathrm{s}}$, $-34°10'50''$ (this last one was first identified by Bohigas et al. 2004).

Fig. 8 displays a series of images showing the ^{12}CO(1−0) emission distribution within the velocity interval $[-10.0, +2.5]\,\mathrm{km\,s^{-1}}$ in steps of $2.5\,\mathrm{km\,s^{-1}}$ covering the whole complex. The images show that the bulk of the molecular gas related to the complex has velocities in the range $[-10.0, 0.0]\,\mathrm{km\,s^{-1}}$, coincident with previous findings by Massi et al. (1997). The most outstanding feature is a CO depression near the centre of the images, encircled by a ring-like structure of strong CO emission easily identified in the range $[-7.5, 0.0]\,\mathrm{km\,s^{-1}}$ (indicated as Shell A in Fig. 8). G353.12+0.86 coincides with the central cavity of Shell A.

In addition to this structure, other molecular clouds are identified in the CO images. These are labelled clouds B to H and appear

to be linked to different nebulosities in the complex. They will be analysed in Sections 4–7.

The large-scale CO emission distribution coincides with areas of high extinction and with the massive dense cores identified by Russeil et al. (2010).

After this general description, we analyse in the next sections the shell G353.12+0.86, the H II region G353.2+0.9 and the large shell.

4 THE SHELL-LIKE FEATURE G353.12+0.86

4.1 The central region of NGC 6357

Two optical shells are apparent near the centre of Fig. 1. They are centred at $17^{\mathrm{h}}24^{\mathrm{m}}35^{\mathrm{s}}$, $-34°14'27''$ and at $17^{\mathrm{h}}25^{\mathrm{m}}13^{\mathrm{s}}$, $-34°16'35''$, respectively. The central cavities and the surrounding envelopes are clearly identifiable in the composite images displayed in Figs 1, 2, 5 and 7. Figs 1 and 7 reveal that the intense Hα emission that delineates the shells is almost completely encircled by emission at 8 μm. A comparison of Figs 1 and 5 shows that both optical shells have radio counterparts.
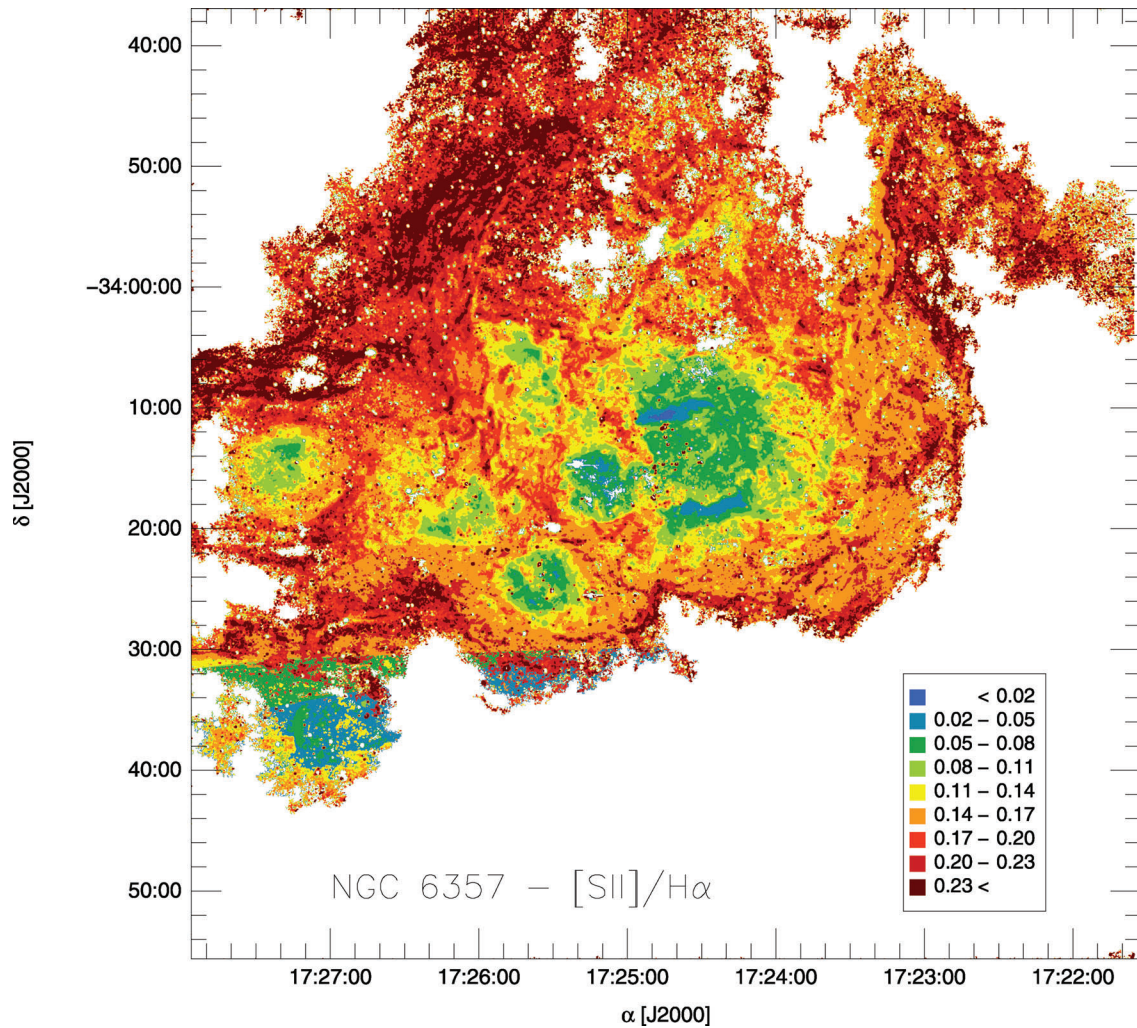
Figure 3. [S II]/Hα line ratio using the images obtained at CTIO. Continuum was subtracted from the individual images. The colour scale is indicated in the lower-right corner of the image. White areas correspond to regions below the cut-off value.

The optical shells are separated by a dust cloud clearly discernible in Fig. 1 (at $17^h24^m55^s$, $-34°14'$). These images suggest that this dust cloud is a foreground object. In this scenario, both shells would be a unique structure with the most massive stars inside.

The CO emission distribution shown in Fig. 8 reveals a region without molecular emission centred at $17^h24^m45^s$, $-34°16'$, coincident with the position of the two optical cavities. As pointed out before, the CO hole is almost completely encircled by molecular gas with velocities in the range of $[-7.5, 0.0]$ km s^{-1} (indicated as Shell A in Fig. 8). A comparison with the optical image clearly shows that these two optical shells are surrounded by molecular material. Thus, the CO emission distribution confirms the presence of PDRs at the interface between the ionized and molecular gases.

A comparison of the distribution of the massive dense cores found by Russeil et al. (2010) with Shell A shows that 65 per cent out of the ∼ 70 massive cores are projected on to the CO shell. Velocities of the most massive cores are in the range of -2.0 to -4.3 km s^{-1}, in agreement with the velocity of Shell A. This indicates that the molecular counterpart of G353.12+0.86 is a region of active star formation that has probably been triggered by the expansion of G353.12+0.86 (see for example Dester & Desch 2005).

The dust column that separates the optical shells can be identified as an elephant trunk pointing towards the centre of G353.12+0.86. The dust cloud coincides in position with a CO cloud having velocities in the range of $[-12.5, -7.5]$ km s^{-1} (named cloud B in Fig. 8). However, the existence of molecular gas linked to this dust cloud with velocities $v > -7.5$ km s^{-1} cannot be ruled out because of the poor angular resolution of the CO data in comparison with the optical and radio images. Our results are compatible with those by Massi et al. (1997), who found molecular gas linked to this dust cloud with velocities in the range of $[-11.5, -6.5]$ km s^{-1} (the south-eastern complex, SEC). At least four high-density molecular cores listed by Russeil et al. (2010) are projected on to this dust column. For the two most massive cores (#112 and #115 in their table 2) these authors find velocities of -5.19 and -8.43 km s^{-1}, compatible with the velocity of cloud B. The fact that the borders of the dust cloud are ionized, the presence of PAH emission at 8 μm adjacent to the ionized gas (see Fig. 7), and the existence of molecular gas in the region, clearly indicates that molecular gas is being photodissociated by the UV photons of Pis 24.

As pointed out by Massi et al. (1997), the fact that the molecular gas linked to the dust cloud has velocities more negative than the CO associated with Shell A gives additional support to the
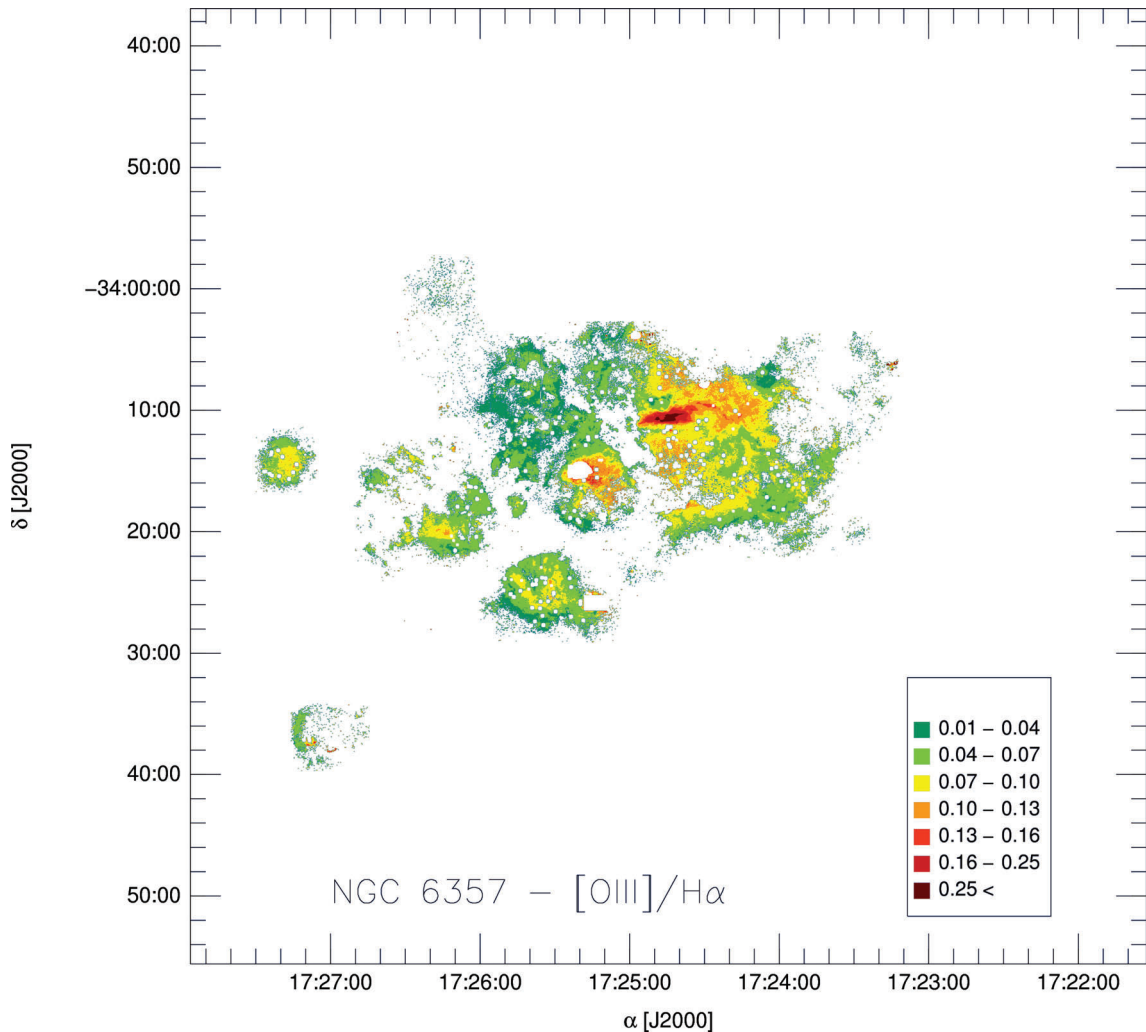
Figure 4. [O III]/Hα line ratio. Continuum was subtracted from the individual images. The colour scale is indicated in the lower-right corner of the image. White areas correspond to regions below the cut-off value.

suggestion that the dust cloud (and cloud B) is in front of the shells. Consequently, the two ionized shells may be one structure ionized by the UV photons of some of the massive stars in Pis 24 and swept up by the strong stellar winds. From here on, this structure of 20×9 arcmin^2 in size (14.5×6.6 pc at 2.5 kpc) will be referred to as G353.12+0.86, Shell A being its molecular counterpart.

The molecular hydrogen column density N_{H_2} and the molecular mass associated with Shell A and cloud B were estimated from the ^{12}CO data, making use of the empirical relation between the integrated emission W_{CO} ($\equiv \int T \, dv$) and N_{H_2}. We adopted $N_{H_2} = (1.9 \pm 0.3) \times W_{CO} \times 10^{20}$ cm^{-2} (K km s^{-1})$^{-1}$, obtained by Murphy & May (1991). The amount of molecular gas in Shell A between -7.5 and 0 km s^{-1} is $(1.2 \pm 0.6) \times 10^5$ M$_\odot$, while for cloud B, we derive $(3.4 \pm 1.7) \times 10^3$ M$_\odot$ taking into account the emission in the range $[-12.5, -7.5]$ km s^{-1}. Velocity intervals and H$_2$ masses of the clouds identified in NGC 6357 are listed in Table 1.

In the following paragraphs we analyse in some detail the characteristics of this structure.

4.2 Morphology and characteristics of G353.1+0.86

The central cavity of G353.12+0.86 shows diffuse [O III] emission revealing that it is filled by hot gas at $T \approx 10^4$ K. The [O III]/Hα ratio

derived for the cavity (in the range of ≈ 0.09–0.12, Fig. 4) indicates a region with high-excitation conditions. Pis 24 is the main excitation source of this shell, since most of its massive stars are seen in projection on to the northern part of the cavity.

The north-western section of the cavity is sharply bounded by the bright H II region G353.2+0.9 (this region is analysed in Section 5).

The western boundary of G353.12+0.86 (near $17^h24^m16^s$, $-34°11'38''$) is thick, with an intricate net of filaments detected in optical lines. The [O III] filaments are located in the inner part of the wall (Fig. 1). The radio continuum image (Fig. 5) displays faint and diffuse emission coincident in position with the area where the [O III] and Hα filaments are distributed. Emission at 8 μm reveals a complex network of filaments, mixed with those observed at Hα (Figs 1 and 7). The emission distribution at different wavelengths in this region suggests that PDRs and optical filaments at different distances along the western wall of the shell are observed.

The south-western rim of the cavity, near $17^h24^m30^s$, $-34°19'$, is sharp and bright in optical lines, in the radio continuum and at 8 μm (Figs 1, 5 and 7). A close inspection of Fig. 1 shows that the emission in the different optical bands does not coincide in position, being the bright [O III] emission closer to the excitation sources than the Hα emission, while the strong [S II] emission is located slightly to the south of the Hα emission. The Hα and the
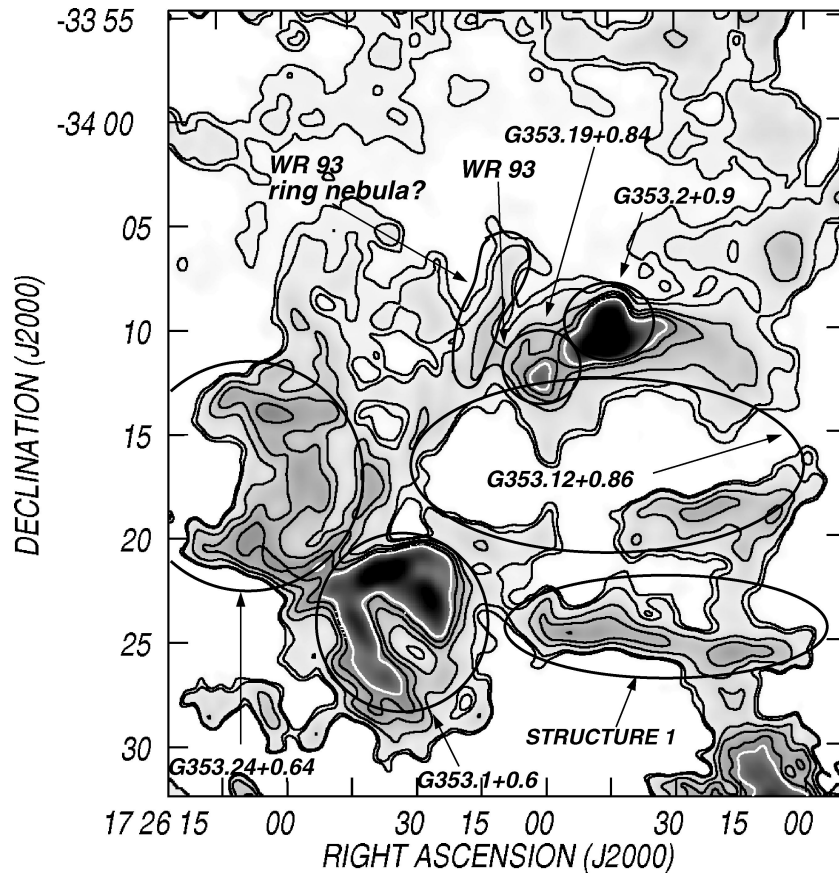
Figure 5. VLA image at 1.46 GHz of the NGC 6357 complex. Grey-scale ranges from -0.01 to 6.6 Jy beam^{-1}. Contours correspond to 0.05, 0.10, 0.30, 0.50, 0.75 and 1.0 Jy beam^{-1}. Identified structures and the position of WR 93 are indicated. The synthesized beam is 43.9×34.3 arcsec^2 at a position angle of $+41°$. The rms noise in the central part of the image is 20 mJy beam^{-1}.

radio continuum emissions are closely coincident. The emission distribution at different wavelengths indicates the existence of an excitation gradient, with the high-excitation regions closer to the massive stars in Pis 24 than the low-excitation ones. The emission at 8 μm reveals a filament lying ≈1.2 arcmin south of the radio emission, indicating that a PDR has developed at the surface of Shell A. Emission at 3.6 and 4.5 μm is also present in these regions (Fig. 9), with the emission at 4.5 μm almost coincident with the Hα emission. The location of the [S ɪɪ] emission farther away from the excitation sources than the Hα emission is typical in PDRs. A similar stratified ionization structure is present at the interface between the ionized gas and the molecular material in the pillars of M 16, where PDRs have developed (Hester et al. 1996).

East of 17^h25^m, the shell displays strong [S ɪɪ] emission encircling the Hα emitting region. No OB stars (see Massey et al. 2001) are known to be projected on to this section of the cavity. Inspection of table 5 by Wang et al. (2007) resulted in the identification of a dozen stars projected on to the cavity. Based on 2MASS colour–colour and colour–magnitude diagrams, these stars are A-type or later.

In summary, the southern, eastern and western edges of G353.12+0.86 show a clear stratification, with the high-excitation ionized gas closer to the massive stars in Pis 24 than the low-excitation ionized gas and the PAHs, pinpointing the last ones the interface between the ionized and molecular gas.

The emission distribution in all the bands displayed in Figs 1, 5 and 7 reveals that the shell is an interstellar bubble blown by the massive stars in the cluster Pis 24. The interstellar gas has been swept up and compressed on to the molecular wall by the stellar

winds of the massive stars in the stellar cluster. The emission distribution resembles some of the IR bubbles described by Watson et al. (2008, 2009).

The physical parameters of the ionized gas were estimated from the image at 1.46 GHz. These values were derived from the expressions by Mezger & Henderson (1967). The ionized mass was multiplied by 1.27 to take into account the contribution of He singly ionized (10 per cent He abundance). We adopted a distance of 2.5 kpc and an electron temperature of 8000 ± 1000 K, in agreement with estimates from radio recombination lines by Wilson et al. (1970) and Quireza et al. (2006). We have taken into account the fact that the plasma is distributed in a shell of width of 1.4 and covers 20 per cent of the area of the shell. The derived values are listed in Table 2, where we include the flux density at 1.46 GHz, the emission measure EM, the size of the structure in arcmin and pc, the rms electron density and the H ɪɪ mass and the ionized mass (including singly ionized He). Errors in electron densities and masses take into account an uncertainty of 20 per cent in distance and about 50 per cent.

5 G353.2+0.9 AND ITS CLOSE ENVIRONS

Fig. 5 reveals that the radio continuum emission in this region is concentrated into two bright clumps: the strongest one coincides with the optically bright region G353.2+0.9 ($17^h24^m47^s$, $-34°10'$), while the other one is centred at (17^h25^m, $-34°12'20''$) (named G353.19+0.84 hereon). A small blister linked to the O6.5V ((f)) star N36 (≡Pis 24+3, Massey et al. 2001) was detected by Bohigas
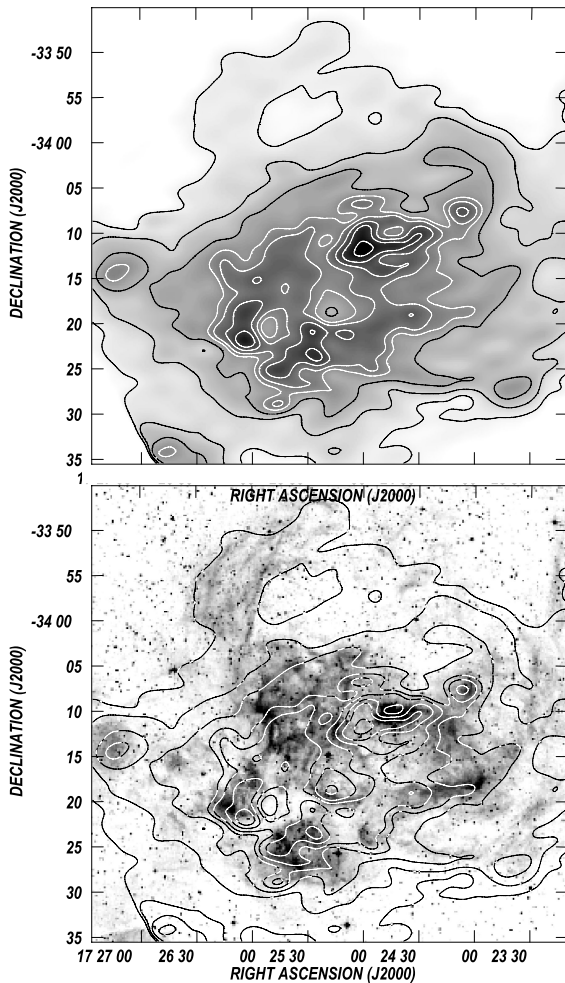
Figure 6. Top panel: dust colour temperature T_c estimated from the *IRAS* images at 60 and 100 μm. Contours range from 33 to 54 K in steps of 3 K. The grey-scale ranges from 33 to 54 K (areas in black correspond to the highest temperatures). The image was smoothed to 2 arcmin. Bottom panel: overlay of the dust colour temperature (contours) and the Hα emission (grey-scale).

et al. (2004) inside G353.2+0.9. In the following subsections, we analyse the H II region G353.2+0.9, the small blister linked to N36 and G353.19+0.84.

5.1 G353.2+0.9

A comparison between Figs 1 and 5 suggests that Hα and [O III] emissions correlate with the radio emission. The sharp southern boundary detected both at optical lines and in the radio continuum suggests that the ionized gas is being pushed by the massive stars in Pis 24, located close to the southern border of the bright region (Bohigas et al. 2004). The emission distribution at 8 μm shows PAH emission in the IRAC 8-μm band projected on to the bright H II region (white area in Fig. 7).

Fig. 9 displays an enlargement of this region in the IRAC bands at 3.6 (in blue), 4.5 (in green) and 8 μm (in red). The southern border of G353.2+0.9 is very bright at 4.5 and 8 μm (area in orange). Emission at 4.5 μm, detected in the southern area may originate in shocked gas. The elephant trunk detected at $17^h24^m45^s$, $-34°10'55''$ in optical data by Bohigas et al. (2004), which points directly towards the open cluster, radiates in the PAH features. The southern

border of G353.2+0.9 and the pillar were analysed in detail by Wesmoquette et al. (2010), who found kinematical evidence of a strong interaction between Pis 24 and the gas in the pillar. Fig. 6 shows that the dust colour temperature in this region (near $17^h25^m45^s$, $-34°12'$) is higher than expected for an H II region, which is compatible with a region where shock and ionization fronts are present.

Fig. 8 shows the existence of molecular gas probably related to this H II region with velocities in the range of $[-7.5, +2.5]$ km s^{-1}. This material partially overlaps the H II region, extending to the north (cloud C in Fig. 8). CO gas at negative velocities is clearly interacting with the nebula, while material at positive velocities seems to be located behind the ionized gas, in agreement with the detection of PAH emission superimposed to the ionized region. These results coincide with those by Massi et al. (1997), who found molecular gas with peak velocities at -6 km s^{-1} to the north and north-east of the nebula, and at -2 km s^{-1} located behind the ionized gas, and with Russeil et al. (2010), who detected dense molecular cores with similar velocities (-3.9 and -5.6 km s^{-1}). The fact that the ionized region is very bright in optical lines is compatible with most of the dense molecular gas being to the north or behind the nebula, in agreement with previous findings by Bohigas et al. (2004) and Wang et al. (2007). The molecular gas distribution confirms the previous suggestion by Bohigas et al. that the region is ionization bounded.

The amount of molecular gas in the components peaking at -6 and -2 km s^{-1} (which cannot be separated in our data set and correspond to cloud C), as estimated from our CO data, is $(2.4 \pm 1.2) \times 10^4$ M$_\odot$.

The physical parameters of the ionized gas, including electron densities and ionized masses derived from our radio continuum image, are summarized in Table 2. We have adopted a background emission of 0.5 Jy beam^{-1} to perform these estimates, and an electron temperature of 9500 K (Bohigas et al. 2004). The ionized mass is similar to that estimated by Bohigas et al. (2004). Electron densities obtained by those authors from line ratios are about 2000 cm^{-3}, higher than our estimates (410 cm^{-3}). An estimate of the filling factor f can be obtained as $f = \sqrt{n_{radio}/n_{opt}}$, where n_{radio} is the rms electron density derived from radio data, and n_{opt} is the local electron density estimated from line ratios, which is more sensitive to higher density regions. This parameter indicates the volume of the H II region that is really occupied by plasma. The derived value is $f \approx 0.5$ and suggests that ionized gas is present in most of the volume of this region.

5.2 The blister related to N36

The presence of a small cavity created by the O6.5V ((f)) star N36 ($17^h24^m45^s.68$, $-34°9'39''.9$, with an optical extinction of about 6.5 mag) inside the brightest section of G353.2+0.9, at $17^h24^m46^s$, $-34°9'50''$, is evident in the [O III] and [S II] images, and in the ratio images, mainly in the [O III]/Hα image (Fig. 4).

The cavity was already detected by Bohigas et al. (2004) and Wang et al. (2007). The value of the [O III]/Hα ratio changes sharply from about 0.1 in the periphery to about 0.25 at the centre of the blister. The [S II]/Hα line ratio, which is almost uniform across the whole region, suggests that the change in the [O III]/Hα ratio is mainly due to local extinction.

Fig. 9 reveals a complex net of filaments at 3.6 and 8 μm (areas in magenta), which also depicts diffuse emission at 4.5 μm. Most of these concentric filaments seem to have a common centre, located close to the position of N36. Small dust regions are also detected in connection with these filaments.
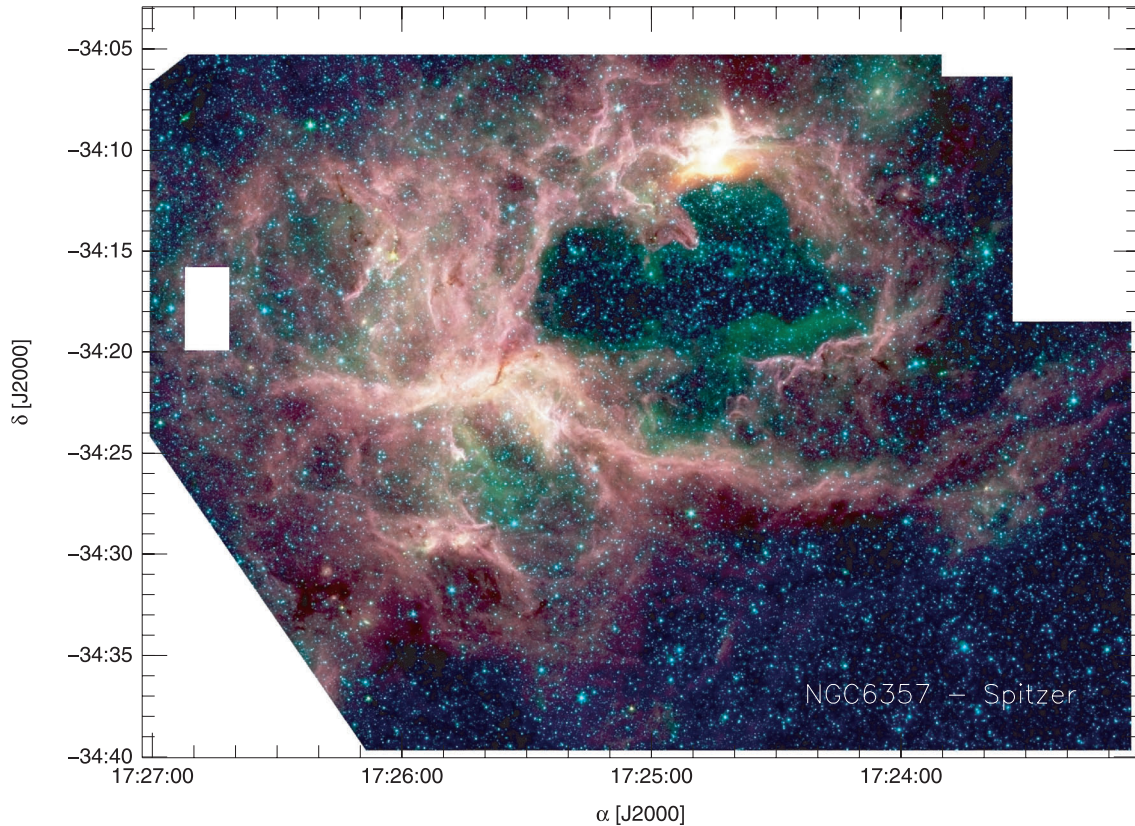
Figure 7. Composite image of the central region of NGC 6357 using IRAC images: 3.6 μm is in blue, 4.5 μm in green and 8 μm in red.

The cavity around N36 can also be identified in the 5-GHz VLA image obtained with a synthesized beam of 3.5 arcsec by Felli et al. (1990). Our VLA image is consistent with these findings, since the area of highest radio emission is projected towards the south of the blister.

5.3 G353.19+0.84

The emission at 1.46 GHz extends to the south-east of G353.2+0.9, where an ionized clump whose brightest section is centred at $17^h25^m00^s$, $-34°12'20''$ can be identified (Fig. 5). This clump was barely detected in the image at 5 GHz obtained by Felli et al. (1990) as a small region of low emission. It cannot be identified at optical lines (Fig. 1).

This ionized region is behind an area of strong visual absorption described in Section 4). The ionized clump is projected on to a ring of PAH emission evident in both Figs 4 and 9. The emission in the far-IR at 60 μm (not shown here) is relatively strong in all the area. These facts suggest that cold and large interstellar grains are mixed with the ionized gas, where PAHs are destroyed.

Part of cloud B, detected in the range [−12.5,−7.5] km s^{-1}, may be either linked to this ionized clump or located in front of it.

A striking elephant trunk pointing towards Pis 24 appears projected on to the southern border of this radio source (at $17^h24^m59.8^s$, $-34°12'50''$). The IR point source located at the top of the pillar ($17^h24^m59.4^s$, $-34°12'49''.8$) might be an evaporating green globule (EGG), as the ones described by Hester et al. (1996).

The existence of a PDR bordering the ionized region cannot be ruled out.

The X-ray source at $17^h24^m55.85^s$, $-34°12'34''.0$ (number 654 in the list by Wang et al. 2007), which has a bright stellar counterpart, lie close to the borders of the strong radio source. The MSX sources G353.1998+00.8506 and G353.2021+00.8313, also projected near the borders of the ionized region, can be classified as MYSOs and CHII, respectively, and might be the excitation sources of this region.

The main physical parameters of the ionized gas in this region are summarized in Table 2. A background emission of 0.3 Jy beam^{-1} and $T_e = 9500$ K were adopted.

Finally, parameters for the whole G353.2+0.9 region including G353.19+0.84, and the low-level emission region that surrounds these sources are also included in Table 2. An electron temperature of 9500 K was assumed.

6 A RING NEBULA RELATED TO WR 93?

The bright WR star HD 157406 (RA,Dec.(J2000) = $17^h25^m08.88^s$, $-34°11'12''.8$) is a probable member of Pis 24 (Massey et al. 2001). Spectroscopic studies estimate a mass-loss rate of 2.5×10^{-5} M$_\odot$ yr^{-1} and a wind terminal velocity of 2290 km s^{-1} for the star (Prinja, Barlow & Howarth 1990; van der Hucht 2001). With these parameters, it is expected that the massive star will deeply perturb the surrounding gas.

The star is projected close to a bright filament seen in optical lines and in the radio continuum at 1.46 GHz, extending from $17^h25^m6^s$, $-34°6'25''$ to $17^h25^m15^s$, $-34°12'$ (the filament is indicated in Figs 2 and 5). The filament is particularly bright in [O III] and was
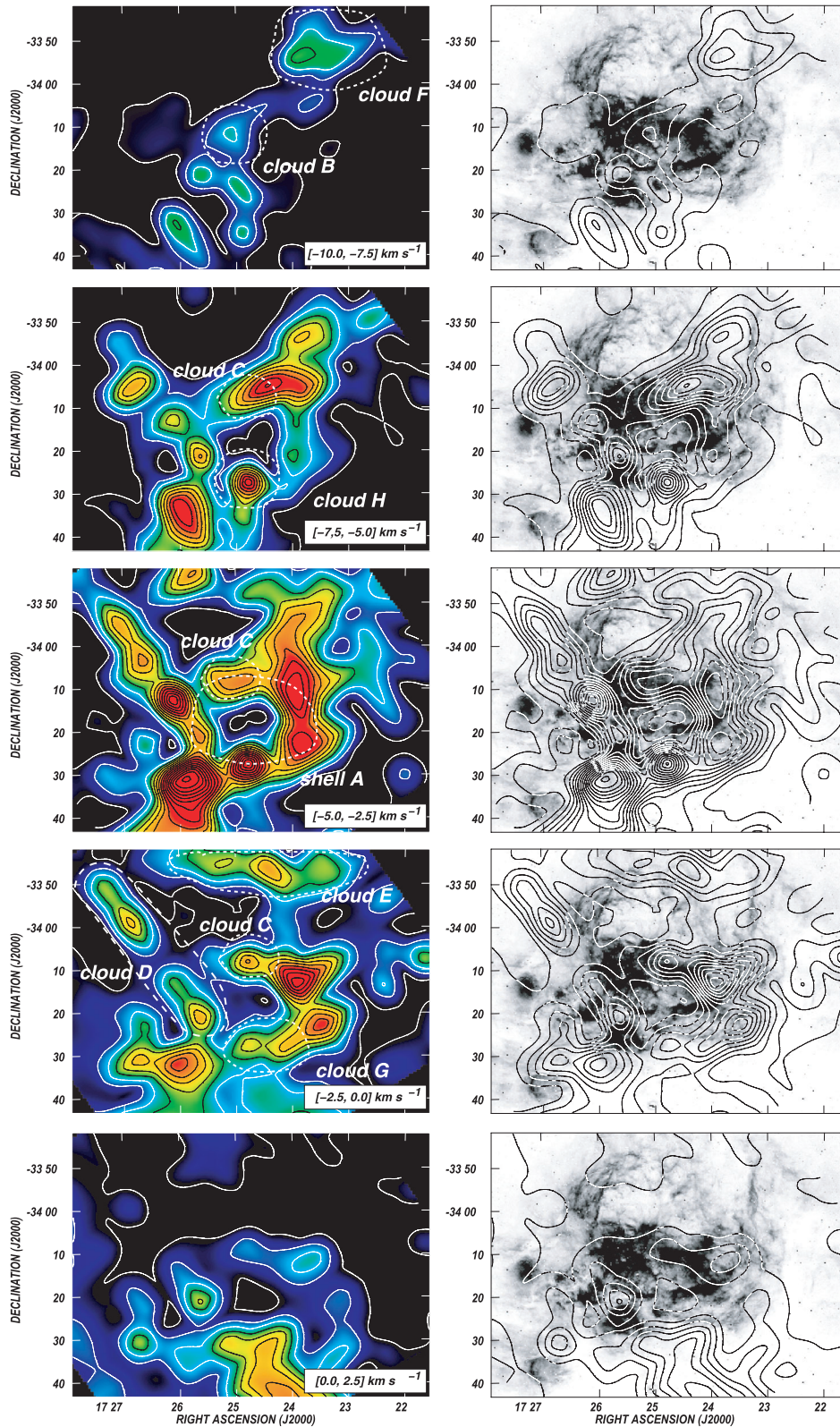
Figure 8. Left panels: ^{12}CO(1−0) emission distribution within the velocity interval [−10.0,+2.5] km s^{-1} in steps of 2.5 km s^{-1}. The velocity interval is indicated in the bottom-right corner of each image. Intensities are expressed as main beam brightness temperature averaged over each velocity interval. Contour levels start at 0.7 K ($\equiv 12.5\sigma$), increasing in steps of 1.75 K. Colour scale goes from 0.7 (dark blue) to 10.5 K (red). The angular resolution of the CO data is 2.6 arcmin. Shell A, as well as clouds B, D, E, F, G and H are indicated only in one map, although they span a larger velocity interval. Right panels: overlay of the same CO contours of the left-hand panels and the Hα image.

Table 1. Physical parameters of the ionized gas.

	$S_{1.46\,GHz}$ (Jy)	EM (10^5 pc cm^{-6})	2R (arcmin)	2R (pc)	n_e (cm^{-3})	$M_{H\,II}$ (M$_\odot$)	M_i (M$_\odot$)	$\log N_{Ly-C}$
G353.12+0.86	34.5	0.7	20×9	14.5×6.6	200	240	330	50.0
G353.2+0.9	41.0	7.8	5.4×3.3	3.9×2.4	410	160	200	49.3
G353.19+0.84	5.0	1.5	4.2×2.9	3.1×2.1	190	40	50	48.5
Whole area[a]	93.6	3.0	14.6×5.4	10.6×3.9	200	710	900	49.7

[a]Includes G353.2+0.9, G353.19+0.84 and lower emission areas.

interpreted as part of a ring nebula related to the WR star (Marston et al. 1994).

The emission at 8.3 μm delineates the eastern border of the filament, reinforcing the suggestion that it is being excited by massive stars located to the W of the filament, where the WR star is located.

The complexity of the gas distribution in NGC 6357, the large number of shells, filaments and dust patches (in particular near the WR star) ensure that the identification of an interstellar bubble created by the strong stellar winds of this star is unlikely.

7 THE LARGE SHELL

The thick E and W arms of the large shell are clearly identified in the composite image of Fig. 1, with the W arm bending to the east near Dec.(J2000) = −34°27′. The ionized filament detected from $17^h23^m30^s$, −34°27′ to approximately 17^h25^m, −34°24′ (named Structure 1 in Figs 2 and 5) is about 13.0×2.0 arcmin^2 in size. The large shell, of about 60 arcmin in size (or 44 pc at 2.5 kpc) open to the north, is mainly detected in Hα emission. Most of the filaments are also easily identified in the faint [S II] emission (e.g. near RA,Dec.(J2000) = $17^h25^m56^s$, −33°25′10″). The [S II] emission is an order of magnitude lower than the Hα emission. The high [S II]/Hα line ratios (>0.17, Fig. 4) of the large shell and the lack of [O III] emission confirm the low-excitation conditions, as previously suggested by Lortet et al. (1984).

A comparison of the CO emission distribution at different velocities (Fig. 6) with the Hα emission shows molecular material probably related to the large shell to the east, north and south of the nebula. The E arm of the large shell appears bounded by CO emission located near $17^h26^m40^s$, −34°5′ with velocities in the range of [−7.5,0] km s^{-1} (cloud D in Fig. 8). This cloud, of about 25 arcmin in length, consists of at least three bright clumps and is projected on to a faint Hα emission region. Many dense cores are projected on to two of these clumps (Russeil et al. 2010). We note that part of the material of the CO clumps may belong to Shell A. The coincidence of the molecular emission region with a region of low optical emission suggests that the molecular gas and the associated interstellar dust are in front of the optical filaments, in agreement with the existence of high extinction regions (Russeil et al. 2010). Due to the relatively small field of view, our radio continuum image does not include the E arm and, consequently, it is not clear if optical emission related to this arm is present behind cloud D.

Towards the north, strong CO emission is also present between −5 and 0 km s^{-1}, at −33°45′, extending from 17^h23^m to $17^h26^m30^s$ (cloud E in Fig. 8), and near 17^h23^m, − 33°56′ in the range of [−12.5,−7.5] km s^{-1} (cloud F in Fig. 8). This material is placed to the north of the optical filaments of the nebula. cloud F probably makes expansion of the ionized gas towards the north difficult.

Structure 1 is detected at 1.46 GHz (Fig. 5) and in Hα and [S II] lines, being brighter at the eastern extreme (at $17^h25^m0^s.5$, −34°24′).

The lack of [O III] emission is compatible with low-excitation conditions. Emission in the IRAC band at 8 μm borders the southern part of Structure 1 (Fig. 7), extending to the east up to $17^h25^m25^s$, −34°23′20″, behind a dust cloud. The strong emission at 8 μm to the south of the ionized gas reveals the existence of a PDR at the interface between the ionized and molecular gas. Structure 1 is projected on to molecular material detected in the range of [−2.5,0] km s^{-1} (cloud G in Fig. 8), at $17^h24^m30^s$, −34°30′. CO velocities coincide with the velocity of the ionized gas (≈ -7 km s^{-1}), as shown by radio recombination line (RRL) observations obtained by Quireza et al. (2006) towards this area.

Strong CO emission with velocities in the range [−12.5,−7.5] km s^{-1} is present at 17^h25^m, − 34°25′ (cloud H). Part of this material is most probably connected to G353.1+0.6.

The amount of molecular gas associated with the large shell was estimated by integrating the CO emission in the velocity interval [−12.5,0] km s^{-1}. A molecular mass of $(5.7 \pm 2.8) \times 10^4$ M$_\odot$ was derived for cloud D, $(4.5 \pm 2.2) \times 10^4$ M$_\odot$ for cloud E, $(9.5 \pm 4.7) \times 10^3$ M$_\odot$ for cloud F, $(2.6 \pm 1.3) \times 10^4$ M$_\odot$ for cloud G and $(3.6 \pm 1.8) \times 10^3$ M$_\odot$ for cloud H. The total amount of molecular gas connected to the outer shell is 1.4×10^5 M$_\odot$.

It is worth mentioning that the angular resolution of the CO data is seven times larger than that of the radio image, thus making the association of CO structures with both optical and radio features difficult.

The origin of the large shell was discussed by Wang et al. (2007). This shell may have originated in the massive stars of Pis 24. We cannot discard the fact that the massive progenitor of the WR star has contributed to the shaping of the outer shell (e.g. Wang et al. 2007).

8 MASSES, DENSITIES AND EXCITATION SOURCES

The UV photons necessary to keep the gas of the different regions in the complex ionized can be estimated from the radio continuum emission. These values were derived using $N_{Ly-C}(10^{48}$ s$^{-1}) = 3.51 \times 10^{-5} n_e^2$(cm$^{-3})R^3$(pc). These results are listed in the last column of Table 2. Taking into account the fact that at 25–50 per cent of the UV photons produced by massive stars are absorbed by interstellar dust in H II regions (Inoue 2001), a photon flux of about $(3–8) \times 10^{50}$ s^{-1} is necessary to maintain G353.12+0.86, G353.2+0.9 and G353.19+0.84 ionized. Ionized gas linked to other regions in the complex was not taken into account.

Bearing in mind photon flux estimates by Martins, Schaerer & Hillier (2002) and Vacca, Garmany & Shull (1996), the massive stars in Pis 24 can supply a UV photon flux of $(1.4–3.3) \times 10^{50}$ s^{-1}. Although the massive stars in Pis 24 are major contributors to the ionization of the nebula, in agreement with Massi et al. (1997) and Bohigas et al. (2004), additional massive stars should be identified in NGC 6357 to explain the ionization of the gas in the whole complex.
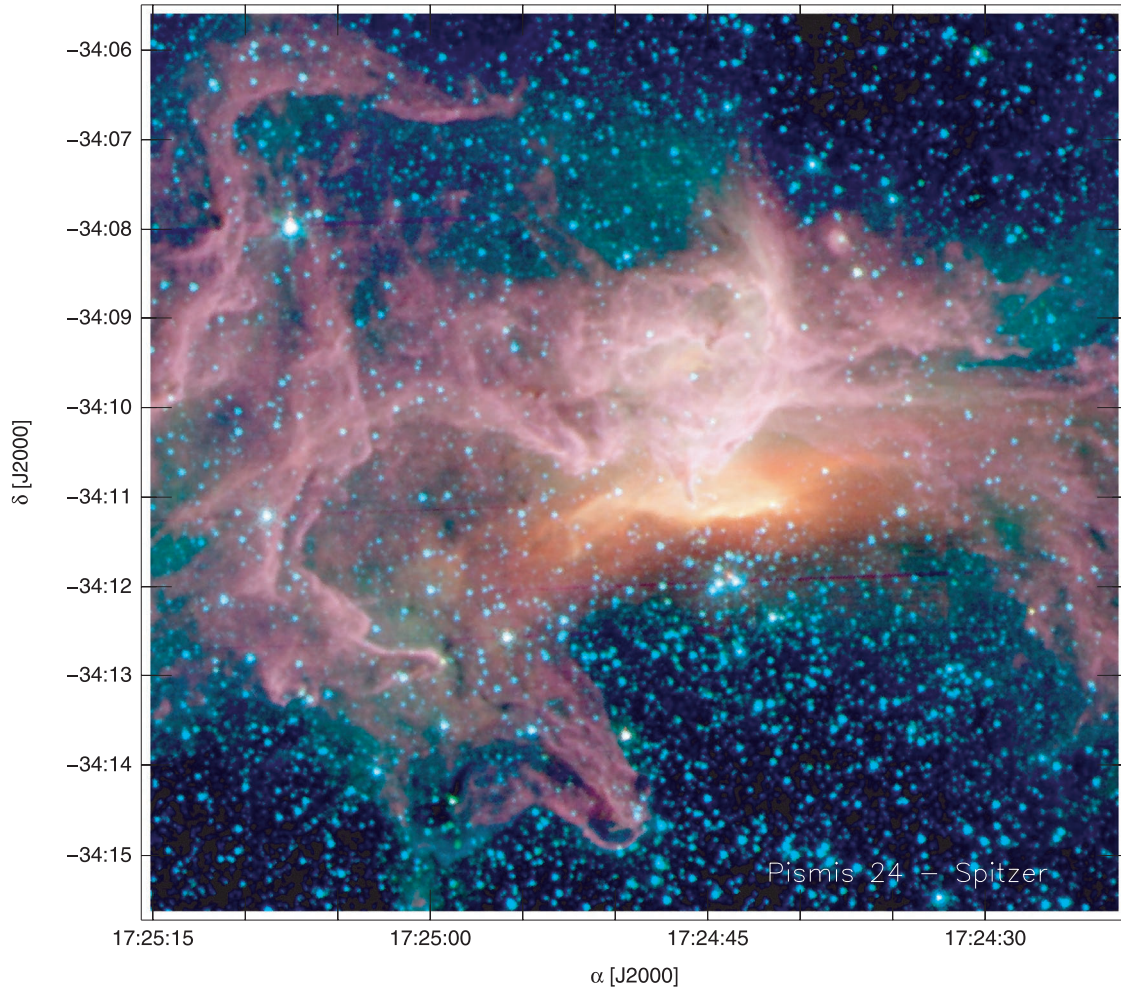
Figure 9. Enlargement of the G353.2+0.9 region as shown by the emission in the IRAC bands: 3.6 μm is in blue, 4.5 μm in green and 8 μm in red.

Table 2. Parameters of the molecular gas.

	(v_1, v_2) km s^{-1}	M_{H2} 10^3 M$_\odot$
Shell A	−7.5,0.0	120 ± 60
Cloud B	−12.5,−7.5	3.4 ± 1.7
Cloud C	−7.5,+2.5	24 ± 12
Outer shell		
Cloud D	−7.5,0.0	57 ± 28
Cloud E	−5.0,0.0	45 ± 22
Cloud F	−12.5,−7.5	9.5 ± 4.2
Cloud G	−2.5,0	9 ± 4
Cloud H	−12.5,−7.5	3.6 ± 1.8

An estimate of the total molecular hydrogen mass involved in the complex can be derived by integrating the CO emission in the range of $[-12.5, +5.0]$ km s^{-1}, within the region displayed in Fig. 9. This value turns out to be $(4 \pm 2) \times 10^5$ M$_\odot$. Our estimate also includes molecular gas linked to G353.1+0.6 and G353.24+0.64.

9 SUMMARY

In this paper we have investigated the distribution of the ionized, neutral gas, and interstellar dust towards NGC 6357. Our goal was

to study the interplay between the massive stars in the open cluster Pis 24 and the surrounding interstellar matter.

The distribution of the ionized gas was analysed using narrow-band Hα, [S ii] and [O iii] images obtained with the Curtis–Schmidt Camera at CTIO (Chile), and radio continuum observations at 1465 MHz taken with the VLA with a synthesized beam of 40 arcsec. The distribution of the molecular gas and of the interstellar dust were studied using ^{12}CO(1−0) data obtained with the NANTEN radiotelescope, Chile, and near- and mid-IR data from the GLIMPSE and *IRAS* surveys, respectively.

NGC 6357 consists of a large ionized shell and numerous smaller shell-like features, dust lanes, globules and elephant trunks. [S ii]/Hα and [O iii]/Hα line ratios provide the evidence to distinguish among H ii regions, interstellar bubbles, and PDRs. Thus, this study revealed new interstellar bubbles surrounded by photodissociation regions in the complex. Molecular observations allowed us to identify the molecular counterparts of the ionized structures in the complex and to confirm the presence of photodissociation regions.

The shell G353.12+0.86 is located near the centre of the complex. It is 15.0 × 6.8 arcmin^2 pc in size at the adopted distance of 2.5 kpc. The shell is detected in Hα and [S ii] emission, as well as in the radio continuum at 1.46 GHz. The [O iii] emission reveals that it is filled by hot gas at 10^4 K. PAH emission surrounds the ionized gas emission, indicating the presence of PDRs. A shell of molecular gas was identified in the CO emission distribution, confirming the

presence of PDRs. A number of dense cores coincide with the CO shell, indicating that the shell is an active region of star formation, probably triggered by the expansion of G353.12+0.86.

The dust column that appears to separate the optical shell in two independent structures is most probably a foreground object. The difference in velocity between the molecular gas associated with the dust column (in the range $[-12.5, -7.5]$ km s^{-1}) and the molecular gas linked to G353.12+0.86 (in the range $[-7.5, 0.0]$ km s^{-1} strongly reinforces this interpretation. In this scenario, G353.12+0.86 is a unique structure with the massive stars of the open cluster Pis 24 inside. The emission distribution in the optical, IR, and radio bands show that this structure is an interstellar bubble blown by the massive stars of Pis 24. The interstellar gas has been swept-up and compressed on to the molecular wall.

G353.2+0.9 is the brightest region at optical, IR, and radio wavelengths. The fact that G353.2+0.9 is very bright both in radio continuum and in optical lines is compatible with the location of most of the dense molecular gas to the north or behind the nebula, confirming the previous suggestion by Bohigas et al. (2004) that the region is ionization bounded. Electron densities derived from our radio continuum image show that this is the region with the highest rms electron density in the complex. An estimate of the filling factor suggests that ionized gas occupies most of the volume of this region.

The synthesized beam of the radio continuum image allowed us to detect the ionized clump G353.19+0.84, 3.1×2.1 pc in size, located slightly to the southeast of G353.2+0.9. This ionized clump is behind an area of strong visual absorption and cannot be detected in optical lines. It can be identified in the far-IR emission and is partially projected on to a ring of PAH emission. These characteristics suggest that large interstellar grains are mixed with the ionized gas, where PAHs are destroyed. Two MSX point sources classified as massive young stellar object and compact H II region might be the excitation sources of this region. A striking elephant trunk pointing towards Pis 24 appears projected on to the southern border of this radio source.

The action of the WR star HD 157504 on the surrounding gas was also investigated. The star may be linked to a bright filament seen in optical lines and in the radio continuum emission. The complexity of the gas distribution near the position insures that the identification of an interstellar bubble created by the strong stellar winds the WR star is unlikely.

The large shell, with a diameter of 44 pc at 2.5 kpc, opens to the north. It is detected in Hα and [S II] emissions. The high [S II]/Hα line ratios and the lack of [O III] emission confirm the low-excitation conditions. Molecular gas having velocities in the range $[-12.5, +5.0]$ km s^{-1} appears related to the eastern, northern and southern sections of the shell. The total amount of molecular gas connected to the large shell was estimated as 1.4×10^5 M$_\odot$. The massive progenitor of the WR star have probably contributed to the shaping of the large shell.

Mean electron densities derived from the radio data suggest electron densities excess 200 cm^{-3}, indicating that NGC 6357 is a complex formed in a region of high ambient density. The total molecular hydrogen mass involved in the complex is estimated as $(4 \pm 2) \times 10^5$ M$_\odot$.

Estimates of the UV photon flux emitted by the massive stars of Pis 24 indicate that they are the main contributors to the ionization of the nebula. However, additional massive stars should be identified in NGC 6357 to explain the ionization of the gas.

REFERENCES

Benjamin R. A. et al., 2003, PASP, 115, 953
Bohigas J., Tapia M., Roth M., Ruiz M. T., 2004, AJ, 127, 2826
Cesarsky C. J. et al., 1996, A&A, 315, L32
Churchwell E., Povich M. S., Allen D., Taylor M. G., Meade M. R., Babler B. L., Indebetouw R., Watson C., 2006, ApJ, 649, 759
Cichowolski S., Pineault S., Arnal E. M., Testori J. C., Goss W. M., Cappa C. E., 2001, AJ, 122, 1938
Damke G., Barbá R., Morrell N. I., 2006, Rev. Mex. Astron. Astrofís. Conf. Ser., 26, 180
Fazio G. G. et al., 2004, ApJS, 154, 10
Felli M., Persi P., Roth M., Tapia M., Ferrari-Toniolo M., Cervelli A., 1990, A&A, 232, 477
Haynes R. F., Caswell J. L., Simons L. W. J., 1978, Australian J. Phys. Astrophys. Suppl., 45, 1
Hester J. J., Desch S. J., 2005, in Krot A. N., Scott E. R. D., Reipurth B., eds, ASP Conf. Ser. Vol. 341, Chondrites and the Protoplanetary Disk. Astron. Soc. Pac., San Francisco, p. 107
Hester J. J. et al., 1996, AJ, 111, 2349
Hildebrand R. H., 1983, QJRAS, 24, 267
Inoue A. K., 2001, AJ, 122, 1788
Kutner M. L., Ulich B. L., 1981, ApJ, 250, 341
Lortet M. C., Testor G., Niemela V., 1984, A&A, 140, 24
Maíz Apellániz J., Walborn N. R., Morrell N. I., Niemela V. S., Nelan E. P., 2007, ApJ, 660, 1480
Marston A. P., Yocum D. R., Garcia-Segura G., Chu Y.-H., 1994, ApJS, 95, 151
Martins F., Schaerer D., Hillier D. J., 2002, A&A, 382, 999
Massey P., DeGioia-Eastwood K., Waterhouse E., 2001, AJ, 121, 1050
Massi F., Brand J., Felli M., 1997, A&A, 320, 972
McBreen B., Jaffe D. T., Fazio G. G., 1983, AJ, 88, 835
Mezger P. G., Henderson A. P., 1967, ApJ, 147, 471
Murphy D. C., May J., 1991, A&A, 247, 202
Neckel T., 1978, A&A, 69, 51
Penzias A. A., Burrus C. A., 1973, ARA&A, 11, 51
Persi P., Ferrari-Toniolo M., Roth M., Tapia M., 1986, A&A, 170, 97
Prinja R. K., Barlow M. J., Howarth I. D., 1990, ApJ, 361, 607

Quireza C., Rood R. T., Bania T. M., Balser D. S., Maciel W. J., 2006, ApJ, 653, 1226

Russeil D., Zavagno A., Motte F., Schneider N., Bontemps S., Walsh A. J., 2010, A&A, 515, A55

Shaver P. A., Goss W. M., 1970, Australian J. Phys. Astrophys. Suppl., 14, 133

Ulich B. L., Haas R. W., 1976, ApJS, 30, 247

Vacca W. D., Garmany C. D., Shull J. M., 1996, ApJS, 460, 914

van der Hucht K. A., 2001, New Astron. Rev., 45, 135

Walborn N. R. et al., 2002, AJ, 123, 2754

Wang J., Townsley L. K., Feigelson E. D., Getman K. V., Broos P. S., Garmire G. P., Tsujimoto M., 2007, ApJS, 168, 100

Watson C. et al., 2008, ApJ, 681, 1341

Watson C., Corn T., Churchwell E. B., Babler B. L., Povich M. S., Meade M. R., Whitney B. A., 2009, ApJ, 694, 546

Westmoquette M. S., Slavin, J. D., Smith L. J., Gallagher S. J., III, MNRAS, 402, 152

Wilson T. L., Mezger P. G., Gardner F. F., Milne D. K., 1970, A&A, 6, 364

This paper has been typeset from a T_EX/L^AT_EX file prepared by the author.